Ludwig A. Th. Greif, Alexander Mittelstädt, Stefan T. Jagsch, Andrei Schliwa

Twofold gain enhancement by elongation of QDs in polarization preserving QD-SOAs

WISSEN IM ZENTRUM
UNIVERSITÄTSBIBLIOTHEK

Technische
Universität
Berlin

Twofold gain enhancement by elongation of QDs in polarization preserving QD-SOAs

Twofold Gain Enhancement by Elongation of QDs in Polarization Preserving QD-SOAs

L A Th Greif,[*] A Mittelstädt, S T Jagsch, and A Schliwa

Technische Universität Berlin, Institut für Festkörperphysik, Hardenbergstraße 36, 10623 Berlin, Germany

E-mail: lath@physik.tu-berlin.de

Abstract

The impact of quantum dot (QD) elongation on key parameters of QD-based semiconductor optical amplifiers (SOAs) is investigated using a combination of 8-band $\boldsymbol{k} \cdot \boldsymbol{p}$-theory including strain and piezoelectricity up to second order and a rate equation model describing the population of QD ground, excited and wetting layer states. By considering columnar QDs of selected aspect ratios, we show that chip gain and saturation gain can be enhanced by up to $+3.6\,\mathrm{dB}$ via an increased elongation of the individual QDs while retaining polarization preserving amplification and gain recovery times below $700\,\mathrm{fs}$. Our results enable the optimization of polarization preserving QD-SOA devices which combine ultrafast gain recovery with high gain and low power consumption.

Keywords

self-assembled quantum dots, semiconductor optical amplifier, $\boldsymbol{k} \cdot \boldsymbol{p}$-theory, gain enhancement

1 Introduction

Since the first pioneering works predicted most desirable electronic and dynamic properties for quantum dots (QDs),[1,2] they have been in the focus of research for use in semiconductor optical amplifiers (SOAs). Ultrafast gain recovery and pronounced nonlinear effects[3] substantiate the high potential of QD-SOAs in the fields of high frequency signal amplification, all-optical data processing and wavelength conversion using four-wave-mixing (FWM)[4–7]. Devices with modulation frequencies exceeding $200\,\mathrm{GHz}$[8] and a $120\,\mathrm{nm}$ broadband gain with saturation output powers above $20\,\mathrm{dB}$ facilitate wavelength division multiplexing[9,10] and high efficiency symmetric FWM.[11] Furthermore, several experimental and theoretical works have shown that, using closely stacked QDs, polarization preserving amplification can be realized.[12–18] A remaining drawback is the lower chip gain of QD-SOAs when compared to quantum well-based systems, requiring longer or multiple gain devisions to achieve comparable amplification.[9]
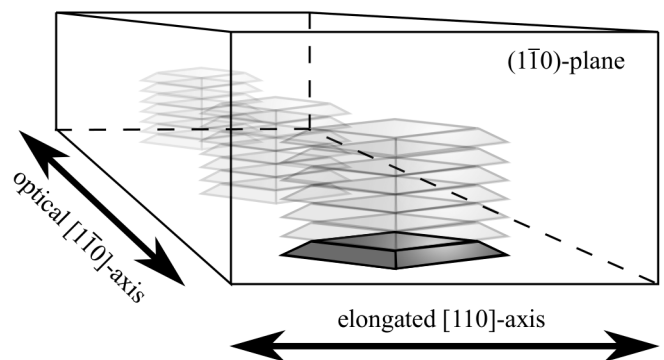

Figure 1: Scheme of the active region of a QD-SOA with closely stacked QDs, showing the axis of elongation with respect to the optical axis.

In this paper, we study an approach to in-

crease the chip gain of a QD-SOA while simultaneously preserving the input signal polarization. The gain enhancement is realized using c-plane QDs that are elongated perpendicular to the optical $[1\bar{1}0]$-axis of the device (figure 1). Several growth studies have demonstrated that such elongated QDs can be realized with molecular beam epitaxy (MBE) as well as metalorganic vapor phase epitaxy (MOVPE) via adjusting the growth temperature or including annealing steps.[19–21] However, the formation of a uniform elongation of all QDs within one stack is still challenging.[22]

Due to the asymmetric confinement in the (001)-plane the QD ground state transition dipole moment is rotated into the $(1\bar{1}0)$-plane, optimizing the alignment with the electric field of the optical signal. Thereby, the polarization of the amplified signal is preserved in the $(1\bar{1}0)$-plane. The results are not limited to this unique configuration of optical axis and QD-axis but can be generalized as long as the axis of elongation is orientated perpendicular to the optical axis of the QD-SOA.

Anisotropic transition dipole moments caused by anisotropic nanostructures were already used in InAs/InP quantum dash lasers and SOAs.[23–25] Quantum dashes represent an intermediate structure between QDs and quantum wires with at least one dimension significantly exceeding the exciton Bohr radius and thus exhibit only two-dimensional quantum confinement.[26] Due to the bigger volume compared to QDs, the threshold current is usually slightly higher than in QD based structures[27] and although polarization insensitive amplification seems achievable[28] to our best knowledge it has not been demonstrated so far.

The paper is organized as follows. After introducing the device structure, a brief paragraph discusses the method for calculating the spatially resolved radiation intensities of a stack of QDs. QD stacks with a vanishing degree of polarization (DOP) in the $(1\bar{1}0)$-plane are then calculated for five different horizontal aspect ratios $AR_{\mathrm{h}} = d_{[110]}/d_{[1\bar{1}0]}$ (elongations), where d_i is the length of the diagonal $[i]$ in the basis plane. Subsequently, the results are used to determine the impact of the QD elongation on the

stimulated emission rate as well as other key properties of the QD-SOA, such as chip gain, saturation gain and gain recovery time (GRT).

2 Structure Details

Typical QD-SOA designs use the tilted ridge waveguide geometry,[5,29,30] where the cross section provides refractive index n guiding along the vertical and gain guiding in lateral direction (figure 2). Following Jayavel et al.,[31] we use $Al_{0.5}Ga_{0.5}As$ for the cladding ($n = 3.1$) and GaAs ($n = 3.3$) as matrix material in order to realize the index guiding.
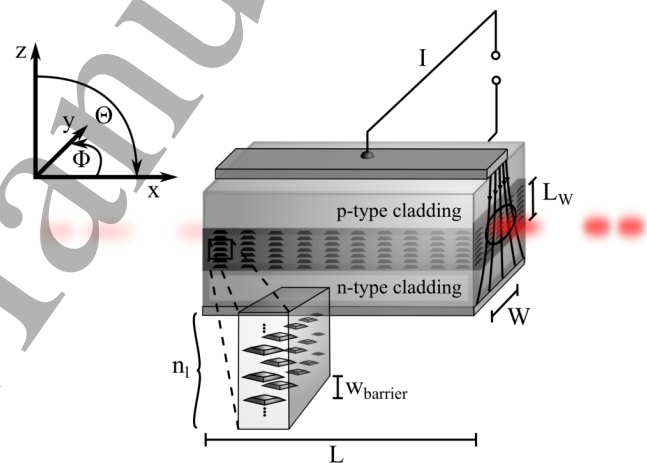
Figure 2: Schematic QD-SOA with pump current I, a resulting current injection region of width W, height of the active region L_{W}, cavity length L and n_{l} layers of quantum dots, each separated by a barrier of width w_{barrier}.

Figure 2 shows the active region composed of seven layers of closely stacked QDs aligned along the c-axis. The QDs are placed on a two-monolayer (ML)-thick wetting layer (included in the QD height). The barrier width w_{barrier} is set to zero ML, as experimental findings suggest that columnar QDs stay in contact with each other along the growth direction.[12,14,15] The individual QDs are modeled as truncated InAs-pyramids with a side-wall angle of $30°$ and dimensions given in table 1.

As shown in [13,32,33], elongation affects the polarization properties of single and stacked QDs. Thus, when changing the QD elongation,

Table 1: Geometric specifications of the individual QDs.

AR_h	QD height	$d_{[110]}$ [nm]
1.0	1.13	12.39
1.5	1.13	11.19
2.0	1.41	12.39
2.5	1.70	12.39
3.0	1.13	7.59

adjustments in the geometry of the individual QDs are necessary to preserve polarization insensitivity of the stacks. Differences in the QD volume are of no particular significance as only the spatial radiation pattern enters the subsequent simulations of the QD-SOA dynamics as discussed in section 3.2.

Device and operational parameters are adapted from [34,35] and listed in table 2.

3 Method of Calculation

In order to connect macroscopic device properties like electric current and photon density with the elongation of the zero dimensional QDs, we use the rate equation model described in [34–37] accompanied by numerically obtained QD emission characteristics. In a first step, the radiation pattern of the QD stacks with different elongations are calculated using an 8-band $\boldsymbol{k \cdot p}$ - model including strain and strain-induced piezoelectricity.[38,39] Subsequently, the radiation pattern is used to determine the ratio of photons spontaneously emitted into the waveguide, known as β-factor

$$\beta = \frac{\text{\# spon. emitted along the waveguide}}{\text{\# all spon. emitted}}.$$
$$(1)$$

This figure of merit enters the rate equation model and allows us to qualitatively study the impact of the QD elongation on the device properties via its influence on the electron and hole wavefunctions.

3.1 Beta-Factor and Spontaneous Emission Rate

In order to obtain the rate of photons emitted by the QDs within the waveguide structure, we use Fermi's golden rule

$$\Gamma_{i \to f}(\boldsymbol{\epsilon}) \propto |\boldsymbol{\epsilon} \cdot \langle f| \boldsymbol{\nabla} |i\rangle |^2. \qquad (2)$$

The polarization dependent transition rate $\Gamma_{i \to f}(\boldsymbol{\epsilon})$ can be derived with the help of the 8-band $\boldsymbol{k \cdot p}$ electron and hole wavefunctions $|f\rangle$ and $|i\rangle$, respectively. Following [40], $\Gamma_{i \to f}(\boldsymbol{\epsilon})$ is transformed into a function of the propagation direction $\boldsymbol{k}$. Only photons whose propagation direction $\boldsymbol{k}(\phi_k, \theta_k)$ fulfills the following equations[41] are confined within the waveguide

$$\theta_k \leq \arccos\left(\frac{\hat{n}_2}{\hat{n}_1}\right) = \theta_{\lim}, \qquad (3)$$

$$\phi_k \leq \arctan\left(\frac{W}{2(L-x)}\right) = \phi_{\lim}. \qquad (4)$$

Here, $\hat{n}_1$, $\hat{n}_2$ are the refractive index of the matrix and cladding material, respectively, W is the width of the injection region, L is the SOA length and x is the position in the SOA along the optical axis. We eliminate the spatial dependence of (4) by averaging the limit angle $\phi_{\lim}$ over the active region

$$\bar{\phi}_{\lim} = \frac{1}{L} \int_0^L dx\, \phi_{\lim}(x). \qquad (5)$$

With the help of the calculated limit angles, the β-factor can be derived as the ratio of the sum of all photons emitted within the limit angles to the total sum of emitted photons.

3.2 Rate Equation Model

The rate equation model is adapted from [34,35,37] with corrections suggested by Li and Li in [36]. The model describes the temporal evolution of the charge carrier densities within the wetting layer N_W, the QD excited state $N_2 = \tilde{N}_Q n_2$ and ground state $N_1 = \tilde{N}_Q n_1$. Here, n_2 and n_1 are the occupation probabilities of excited state and ground state, respectively. Occupation probabilities and carrier

3

densities are connected to the QD volume density $\tilde{N}_Q = N_Q/L_W$ via the QD surface density N_Q.

Lifetimes for the capture $\tau_{W\to 2}$ and intradot relaxation $\tau_{2\to 1}$ are calculated considering phonon-mediated and Auger processes [42]

$$\tau_i = \frac{1}{A_i + C_i N_W} \ , \quad i = (W \to 2), (2 \to 1), \tag{6}$$

where A_i and C_i are the coefficients of phonon- and Auger-assisted interaction, respectively. The lifetimes are connected to the excitation $\tau_{1\to 2}$ and escape process $\tau_{2\to W}$ via a quasi-Fermi equilibrium condition [42] at $T = 300\,\mathrm{K}$,

$$\tau_{2\to W} = \tau_{W\to 2}\frac{2\rho_2 N_Q h^2}{4\pi m_e^* k_B T}\exp\left(\frac{E_W - E_2}{k_B T}\right), \tag{7}$$

$$\tau_{1\to 2} = \tau_{2\to 1}\frac{\rho_1}{\rho_2}\exp\left(\frac{E_2 - E_1}{k_B T}\right). \tag{8}$$

Here, ρ_1 and ρ_2 denote the ground and excited state degeneracy without spin, h is the Planck constant, m_e^* is the effective electron mass, k_B is the Boltzmann constant and E_W, E_2, E_1 are the energies of the wetting layer, excited and ground state. For the considered wetting layer carrier concentrations N_W the relaxation and excitation processes are mainly phonon- ($N_W < 1\mathrm{e}17\,\mathrm{cm}^{-3}$) or Auger-assisted ($N_W > 1\mathrm{e}17\,\mathrm{cm}^{-3}$), while the escape and capture processes are dominated by phonon creation/annihilation, showing nearly no N_W dependence (figure 3). Considering the internal losses α_{int}, the optical power within the SOA can be calculated with the propagation equation [43]

$$P(z) = P_{in}\exp((g - \alpha_{int})z). \tag{9}$$

The dependence of the modal gain g on the ground state occupation probability n_1 can be written as $g = g_{max}(2n_1 - 1)$.[43] In various studies g_{max} is treated as a constant parameter depending only on structural properties of the specific device.[34–36] As we want to compare QD-SOAs with differently elongated QDs, a description of g_{max} as function of the elongation, or ef-
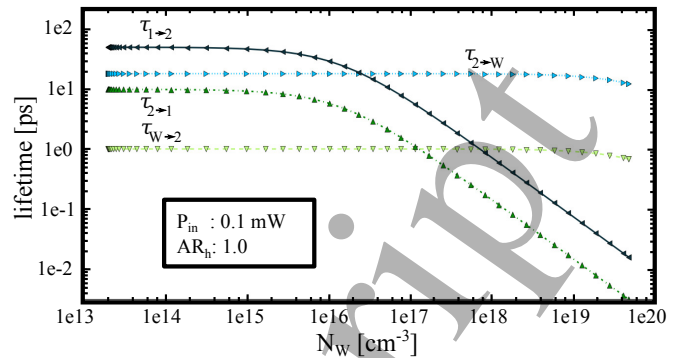
Figure 3: Lifetimes of capture (W→2), relaxation (2→1), escape (2→W) and excitation (1→2) processes for different wetting layer carrier concentrations N_W.

fectively as function of the β-value, is necessary. Following the microscopic derivation of g_{max} in [43,44] a linear dependence on β is revealed. Defining g_{max}^0 for a QD-SOA with unelongated QDs the rate equation model is given as

$$\frac{\partial N_W}{\partial t} = \frac{J}{eL_W} + \frac{N_2}{\tau_{2\to W}} - \frac{N_W(1 - n_2)}{\tau_{W\to 2}} - \frac{N_W}{\tau_{WR}}, \tag{10}$$

$$\frac{\partial N_2}{\partial t} = \frac{N_W(1 - n_2)}{\tau_{W\to 2}} + \frac{N_1(1 - n_2)}{\tau_{1\to 2}} - \frac{N_2}{\tau_{2\to W}} - \frac{N_2(1 - n_1)}{\tau_{2\to 1}}, \tag{11}$$

$$\frac{\partial N_1}{\partial t} = \frac{N_2(1 - n_1)}{\tau_{2\to 1}} - \frac{N_1(1 - n_2)}{\tau_{1\to 2}} - \frac{N_1 n_1}{\tau_{1R}} - \frac{g_{max}^0 \beta (2n_1 - 1)\bar{P}}{\beta_0 \sigma h\nu}, \tag{12}$$

with the injection current density $J = I/(L\,W)$, the elementary charge e, the thickness of the active layer L_W, the radiative lifetime in the wetting layer and GS, τ_{WR}, τ_{1R}, the spatial average of the optical power within the SOA $\bar{P}$, the total cross section of the QDs $\sigma = V_{QDs}/L$, with the total volume of the QDs V_{QDs}.[36]

Equations (10)-(12) are solved using the fourth-order Runge-Kutta method and an incremental time step of $1\mathrm{e}{-4}\,\mathrm{ps}$ except for

Table 2: Parameters used in the rate equation model and the lifetime calculation.

parameter	physical meaning	value
I	injection current	2e-7 A - 20 A
L_{W}	thickness of effective active layer	200 nm
L_{WL}	thickness of wetting layers	3.5 nm
L	length of the SOA	2 mm
W	width of current injection region	10 μm
N_{Q}	surface QD density	5e10 cm^2
$A_{\mathrm{W}\to 2}$	phonon assisted trans. coeff.	1e12 s^{-1}
$C_{\mathrm{W}\to 2}$	Auger assisted trans. coeff.	1e-14 m^{3}s^{-1}
$A_{2\to 1}$	phonon assisted trans. coeff.	1e11 s^{-1}
$C_{2\to 1}$	Auger assisted trans. coeff.	7e-12 m^{3}s^{-1}
ρ_2	ES degeneracy (w/o spin)	2
ρ_1	GS degeneracy (w/o spin)	1
m_{e}^*	effective electron mass	0.0223 m_{e}
$E_{\mathrm{W}} - E_2$	energy splitting W $\to$ 2	80 meV
$E_2 - E_1$	energy splitting $2 \to 1$	60 meV
τ_{WR}	spon. radiative lifetime in wetting layer	10 ps
τ_{1R}	spon. radiative lifetime in GS	400 ps
α_{int}	internal losses	3 cm^{-1}
g_{max}^0	modal gain of a QD-SOA with unelongated QDs	11.5 cm^{-1}

the gain recovery calculations which were performed with a time step of 1e−5 ps.

Finally, the power of the amplified signal P_{out} is calculated

$$P_{\mathrm{out}} = P_{\mathrm{in}} \exp((g - \alpha_{\mathrm{int}})L), \qquad (13)$$

which defines the chip gain G in dB

$$G = 10 \log_{10}(P_{\mathrm{out}}/P_{\mathrm{in}}). \qquad (14)$$

The absolute energies of all states shift with different elongations as shown in [39]. But considering the more important energy spacings, the bandgap as well as the conduction interband spacing of the ground and first excited state are relatively constant. However, the interband spacing for higher states as well as the energy difference to the wetting layer reservoir is much more complex. This work constitutes a proof of concept and thus we refrain from simulations of the extended wetting layer and also from an explicit treatment of several higher excited states which would introduce a large number of unknown parameters.

In our opinion, such a simplified electronic picture is most suitable to first prove the impact of the elongation onto the basic device dynamics. Thus, except for the β-factor which is directly calculated using the QD stack wavefunction, all parameters are treated as constant for all considered QDs (table 2) with values similar to those used in [34,35].

4   Results

Using single-particle states of the 8-band $\boldsymbol{k \cdot p}$-simulations, the DOP and the β-factor can be determined for each elongation of the stacked QDs. Table 3 shows how the β-factor of the QD stack increases with the elongation of the individual QDs, while maintaining near-isotropic polarization through the stack aspect ratio. The increase of the β-factor is most pronounced for slightly elongated structures between $AR_{\mathrm{h}} = 1.0$ and 1.5 and saturates rapidly for higher aspect ratios. In combination with the monotonous increase of β only a small number of elongations has to be considered to

Table 3: DOP and β-factor of differently elongated QD stacks.

AR_h	DOP	β [‰]
1.0	0.08	1.10
1.5	-0.03	1.30
2.0	-0.01	1.41
2.5	-0.03	1.48
3.0	0.10	1.50

map the qualitative impact of AR_h onto the device properties.

According to (3) and (4), β also depends on the waveguide dimensions as well as the material compositions. Therefore, the β-values may vary for identical QD stacks in a waveguide with different dimensions or refractive index.

4.1 Gain Enhancement

Having shown that we can efficiently tune the β-factor using elongated QDs, we now investigate the influence of the elongation on the chip gain, the GRT and the saturation gain.

In figure 4 the QD occupation probabilities n_2 and n_1 as well as the wetting layer carrier concentration N_W are shown as functions of J and elongation for a constant optical input signal of $0.1\,\mathrm{mW}$. For $J < 0.1\,\mathrm{A/cm^2}$ both QD states exhibit constant occupations. Here, a small N_W below $1e14\,\mathrm{cm^{-3}}$ leads to small capture rates $N_W(1 - n_2)/\tau_{W\to2}$ and a long intradot relaxation time $\tau_{2\to1}$ (figure 3). Thus, the ground state is mainly populated due to the constant input signal, resembling an optically pumped two-level system with a steady state occupation of 0.5. In combination with a negligible excitation process $(1 \to 2)$ n_1 significantly exceeds n_2 $(n_2 \ll n_1)$.

If N_W is increased via an increased injection current, the QD refilling takes place more efficiently and thus n_2 increases to unity $(n_2 > n_1)$. This point represents the formation of an intradot relaxation bottleneck where n_1 is limited by the finite intradot relaxation time. A larger N_W also causes smaller intradot relaxation and excitation times, changing the dominating mechanism from phonon- to Auger-assisted

(figure 3). Both processes exhibit different N_W dependencies which leads to the formation of a shoulder in n_1 around $J = 10\,\mathrm{A/cm^2}$. However, the relaxation always exceeds the excitation processes, resulting in a net growth of n_1 with increasing J. Ultimately, both states are completely occupied (upper limit of the relaxation bottleneck) for current densities above $3e4\,\mathrm{A/cm^2}$.

With QD elongation the transition dipole moment is increasingly aligned with the electric field of the propagating optical signal in the $(1\bar{1}0)$-plane. Thus, the rate of stimulated emission increases, reducing n_1. Elongation-induced differences in the occupation probability can solely be observed in the relaxation bottleneck regime for the following reasons.

Firstly, for $J < 0.1\,\mathrm{A/cm^2}$, the ground state is mainly occupied due to the resonant optical signal resembling an optically pumped two-level system. This means that absorption and emission processes exactly compensate each other. Consequently, elongation-induced changes in the rate of stimulated emission do not have any impact on the QD state occupations.

Secondly, for $J > 3e4\,\mathrm{A/cm^2}$, the optical losses are overcompensated by high capture rates and fast intradot relaxation processes. Thus, also in this regime no elongation dependence of n_1 can be found.

In contrast to the QD occupation, the impact of elongation on the chip gain G is not limited to the relaxation bottleneck regime but can be observed as long as $G > 0$ (figure 4 b). Due to the amplified signal-to-QD coupling, the rate of stimulated emission is increased even for identical ground state occupations, leading to an elongation-induced gain enhancement.

Figure 5 a shows the QD occupation as a function of the signal output power. The QD occupation probabilities n_2 and n_1 are calculated for a realistic operating current density of $J = 5e2\,\mathrm{A/cm^2}$ and different QD elongations.[10] For a wide range of output powers $(P_{\mathrm{out}} < 0.1\,\mathrm{mW})$ the occupation is constant for all elongations meaning that the complete inversion of the QD ground states can be preserved $(n_1 = 1)$ due to the fast refilling dynamic on a femto- to picosecond timescale (figure 3).
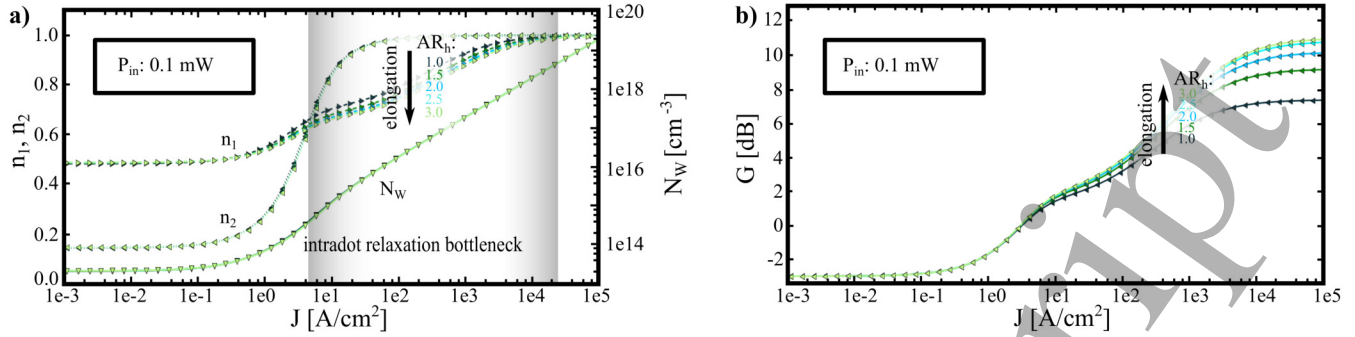
6

Figure 4: **a)** Wetting layer carrier concentration N_W (solid), steady state occupation probabilities of the QD ground state n_1 (dashed) and excited state n_2 (dotted) as well as **b)** chip gain as function of injection current density for QD-SOAs with differently elongated QDs at a signal input power of $0.1\,\text{mW}$.
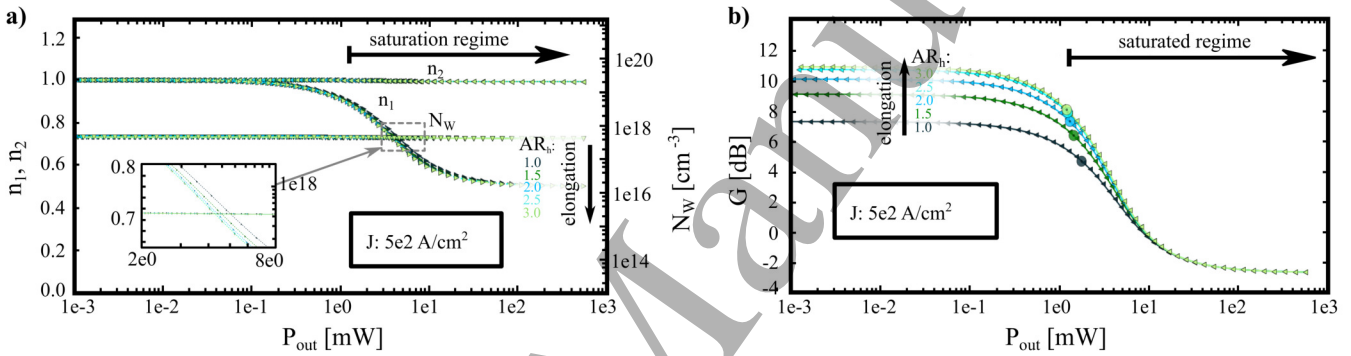

Figure 5: **a)** Wetting layer carrier concentration N_W (solid), steady state occupation probabilities of the QD ground state n_1 (dashed) and excited state n_2 (dotted) as well as **b)** chip gain as function of output power for QD-SOAs with differently elongated QDs at an injection current density of $5e2\,\text{A/cm}^2$. Circles mark the saturation output power and the associated saturation gain.

For output powers in the range of $10\,\text{mW}$ the ground state occupation collapses and is driven into transparency ($n_1 = 0.5$) representing a saturated gain medium. Like in an optically pumped two-level system (figure 4, $J < 0.1\,\text{A/cm}^2$), optical gain and loss processes are compensating each other and, again, n_1 does not depend on the QD elongation. Solely for the transition regime between $0.1\,\text{mW} < P_{\text{out}} < 10\,\text{mW}$ the elongation-dependent increase in signal-to-QD coupling results in slightly reduced occupation probabilities (figure 5 a inset).

For output powers below $0.1\,\text{mW}$, the chip gain as a function of the output power (figure 5 b) provides an elongation-induced gain enhancement of up to $+3.6\,\text{dB}$. These results are in good agreement with an investigation
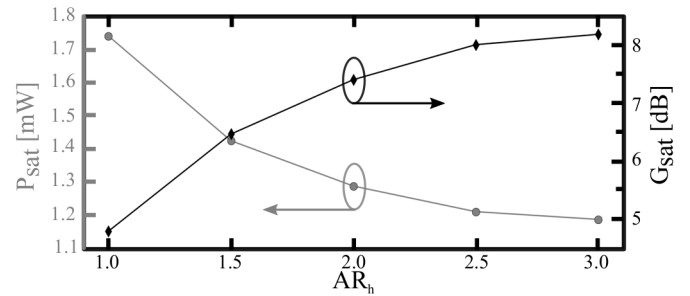

Figure 6: Saturation power (grey circles) and saturation gain (black diamonds) for QD-SOAs with differently elongated QDs.

on quantum dash SOAs whose gain can be increased by $+3.0$ - $4.1\,\text{dB}$ if the optical axis is chosen perpendicular to the quantum dashes, instead of being aligned.[24]

The enhancement is reduced with higher out-

put powers and completely disappears in the saturated regime. In addition to the gain enhancement, the stronger signal-to-QD coupling also shifts the transition to the saturated regime towards lower output powers.

As a figure of merit for this transition the saturation power P_{sat} is calculated, defined as the power for which G is halfway between the low and high power limit[45]

$$P = P_{\mathrm{sat}} \Leftrightarrow G(P) = (G_{\mathrm{low}} + |G_{\mathrm{high}}|)/2 \\ = G_{\mathrm{sat}}. \tag{15}$$

The saturation power and the saturation gain are depicted in figure 5 b and figure 6, respectively, showing that the saturation gain can be enhanced by $+3.4\,\mathrm{dB}$ even though the saturation power decreases with QD elongation. Strikingly, $70\,\%$ ($+2.6\,\mathrm{dB}$) of the maximum gain enhancement can be achieved already for $AR_{\mathrm{h}} = 2$.

4.2 Reduction of Gain Recovery Time

The gain recovery time is analyzed by simulating a monochromatic pump-probe experiment (figure 7).[34,35] To this end, a continuous wave probe signal of variable optical input power monitors the gain collapse and subsequent recovery following a pump pulse. A Gaussian pump pulse with a FWHM of 150 fs and a peak power of 0.01 mW is inserted after the electrically driven system reaches a steady state. The time evolution of the out-coupled probe signal then determines the $(90{:}10)\,\% \ GRT$ as a function of output power and elongation.

The GRT is determined by the competition between the intradot relaxation rate ($\Gamma_{2\to1}$), excitation rate ($\Gamma_{1\to2}$), rate of stimulated (Γ_{stim})
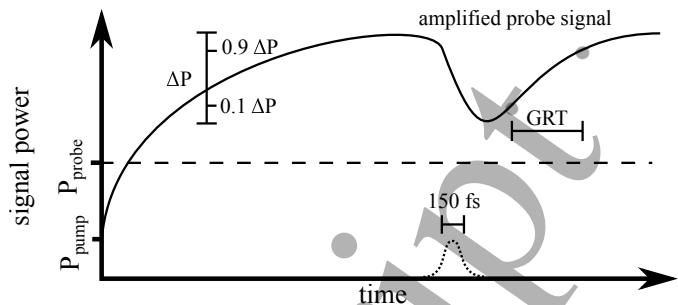

Figure 7: Pump-probe scheme with time evolution of input (pump - dotted; probe - dashed) and amplified probe signal (solid). The amplified probe signal declines by ΔP due to the pump insertion. The time to recover from $10\,\%$ to $90\,\%$ of ΔP defines the GRT.

and spontaneous emission (Γ_{spon})

$$\Gamma_{2\to1} = \frac{N_2(1 - n_1)}{\tau_{2\to1}}, \tag{16}$$

$$\Gamma_{1\to2} = \frac{N_1(1 - n_2)}{\tau_{1\to2}}, \tag{17}$$

$$\Gamma_{\mathrm{stim}} = g_{\mathrm{max}}(2n_1 - 1)\frac{\bar{P}}{\sigma h\nu}, \tag{18}$$

$$\Gamma_{\mathrm{spon}} = \frac{N_1 n_1}{\tau_{1\mathrm{R}}}. \tag{19}$$

Except for the stimulated emission rate, all rates depend on a specific lifetime and QD state occupation probability. While the spontaneous emission lifetime is treated as a constant, the relaxation and excitation lifetimes depend on the wetting layer carrier density (6)-(8).

The lifetimes show no variation with respect to the elongation and only a small step-like increase of up to $11\,\%$ near the saturation power (plots available in supporting informations)

$$\tau_{\mathrm{W}\to2} = 18.25\,\mathrm{ps} \text{ to } 18.26\,\mathrm{ps}, \\ \tau_{2\to\mathrm{W}} = 1.00\,\mathrm{ps}, \\ \tau_{1\to2} = 1.58\,\mathrm{ps} \text{ to } 1.72\,\mathrm{ps}, \\ \tau_{2\to1} = 0.31\,\mathrm{ps} \text{ to } 0.34\,\mathrm{ps}.$$

In contrast, the ground state occupation probability n_1 exhibits an elongation dependence (figure 5 a inset) becoming smaller for increasing elongation and intermediate output powers $0.1\,\mathrm{mW} < P_{\mathrm{out}} < 10\,\mathrm{mW}$. For this reason, the in-scattering rate $\Gamma_{2\to1}$ increases while

the out-scattering rates $\Gamma_{1\to2}$ and Γ_{spon} decrease. Considering the chip gain G for differently elongated QDs as a function of the output power (figure 5 b), we infer that the rate of stimulated emission is increased with elongation as long as P_{out} is lower than $10\,\text{mW}$. Additionally, Γ_{stim} is also proportional to $\bar{P}$ and thus negligible for very low optical powers ($P_{\text{out}} < 0.1\,\text{mW}$).
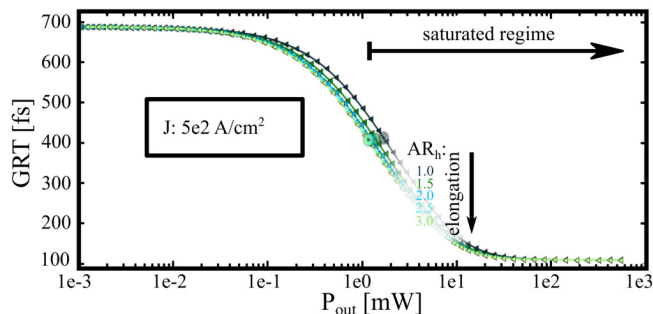

Figure 8: GRT as function of the output power for QD-SOAs with differently elongated QDs. Circles mark the saturation output power and the associated saturation GRT.

Consequently, the GRT as function of optical power and elongation (figure 8) exhibits neither power nor elongation dependence for P_{out} lower than $0.1\,\text{mW}$ or higher than $10\,\text{mW}$. For low optical powers the GRT is significantly longer than the excited state to ground state relaxation time $\tau_{2\to1}$ due to out-scattering processes. This situation is reversed for high optical powers, since high photon absorption rates within the quasi-two-level regime (discussed in section A) result in a GRT much smaller than $\tau_{2\to1}$.

In the intermediate regime, the GRT can be reduced by $60\,\text{fs}$ by increasing AR_{h} from 1 to 3. This reduction is caused by the net increase of the sum of all rates, as the increased losses Γ_{stim} are overcompensated by the elongation-induced increase in in-scattering $\Gamma_{2\to1}$ and the reduced losses $\Gamma_{1\to2}$ and Γ_{spon}.

Analogous to the saturation gain the saturation GRT can be determined $GRT_{\text{sat}} = GRT(P_{\text{sat}})$ (figure 9). In contrast to the GRT for a given output power in the intermediate regime, GRT_{sat} is relatively insensitive to the elongation.
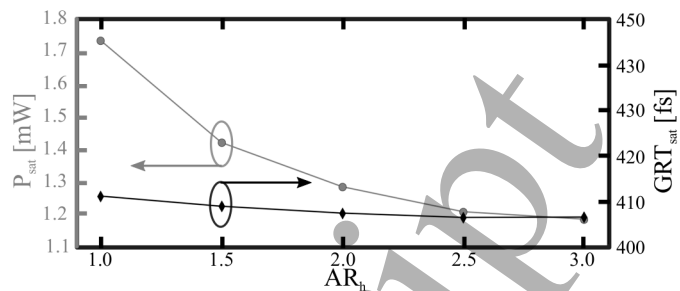

Figure 9: Saturation power (grey circles) and saturation GRT (black diamonds) for QD-SOAs with differently elongated QDs.

5   Conclusion

We have shown how a more than twofold enhancement of both chip gain and saturation gain of a QD-SOAs can be realized when using elongated QDs, while retaining or even improving ultra-fast gain recovery dynamics. Strikingly, a horizontal aspect ratio of 2 already leads to a gain enhancement of $+2.6\,\text{dB}$ representing $70\,\%$ of the overall observed enhancement.

Furthermore, polarization insensitive signal amplification is realized for all elongations through stacking of QDs, forming a vertically coupled confinement region with adjustable emission directionality. As such, our approach makes QD-SOAs more competitive with quantum well-based devices, in particular for applications requiring ultra-fast modulation speeds.

Author Information

Corresponding Author
* lath@physik.tu-berlin.de
ORCID
Ludwig A. Th. Greif:	0000-0002-6732-7062
Alexander Mittelstädt:	0000-0002-7587-9385
Stefan T. Jagsch:	0000-0002-2365-0554
Andrei Schliwa:	0000-0001-7085-3680

Notes

The authors declare no competing financial interest.

Acknowledgement

Supporting Information Available:

Figures of the capture (W→2), escape (2→W), excitation (1→2) and relaxation (2→1) lifetimes as functions of the optical output power for differently elongated QDs.

References

(1) Arakawa, Y.; Sakaki, H. Multidimensional Quantum Well Laser and Temperature Dependence of its Threshold Current. *Appl Phys Lett* **1982**, *40*, 939–941.

(2) Asada, M.; Miyamoto, Y.; Suematsu, Y. Gain and the Threshold of Three-Dimensional Quantum-Box Lasers. *IEEE J Quant Electron* **1986**, *22*, 1915–1921.

(3) Akiyama, T.; Kuwatsuka, H.; Simoyama, T.; Nakata, Y.; Mukai, K.; Sugawara, M.; Wada, O.; Ishikawa, H. Nonlinear gain dynamics in quantum-dot optical amplifiers and its application to optical communication devices. *IEEE J Quant Electron* **2001**, *37*, 1059–1065.

(4) Sugawara, M.; Akiyama, T.; Hatori, N.; Nakata, Y.; Ebe, H.; Ishikawa, H. Quantum-dot Semiconductor Optical Amplifiers for High-Bit-Rate Signal Processing up to 160 Gb/s and a New Scheme of 3 R Regenerators. *Meas Sci Technol* **2002**, *13*, 1683–1691.

(5) Akiyama, T.; Sugawara, M.; Arakawa, Y. Quantum-Dot Semiconductor Optical Amplifiers. *Proc IEEE* **2007**, *95*, 1757–1766.

(6) Ben Ezra, Y.; Lembrikov, B. I.; Haridim, M. Ultrafast All-Optical Processor Based on Quantum-Dot Semiconductor Optical Amplifiers. *IEEE J Quant Electron* **2009**, *45*, 34–41.

(7) Nurmohammadi, T.; Abbasian, K.; As'Adi, M. J.; Jafari, D. Design of an Ultrafast All-Optical NOR Logic Gate Based on Mach-Zehnder Interferometer Using Quantum-Dot SOA. *Optik - Int J Light Electron Opt* **2014**, *125*, 4023–4029.

(8) Matsumoto, A.; Akahane, K.; Sakamoto, T.; Umezawa, T.; Kanno, A.; Yamamoto, N. Dynamic Characteristics of 20-Layer Stacked QD-SOA with Strain Compensation Technique by Ultrafast Signals using Optical Frequency Comb. *Phys Status Solidi A* **2017**, *214*.

(9) Akiyama, T.; Ekawa, M.; Sugawara, M.; Kawaguchi, K.; Sudo, H.; Kuramata, A.; Ebe, H.; Arakawa, Y. An Ultra-Band Semiconductor Optical Amplifier Having an Extremely High Penalty-Free Output Power of 23 dBm Achieved with Quantum Dots. *IEEE Photonic Tech L* **2005**, *17*, 1614–1616.

(10) Matsumoto, A.; Takei, Y.; Matsushita, A.; Akahane, K.; Matsushima, Y.; Ishikawa, H.; Utaka, K. Gain Characteristics and Femto-Second Optical Pulse Response of 1550 nm-Band Multi-Stacked QD-SOA Grown on InP(311)B Substrate. *Opt Commun* **2015**, *344*, 51–54.

(11) Akiyama, T.; Kuwatsuka, H.; Hatori, N.; Nakata, Y.; Ebe, H.; Sugawara, M. Symmetric Highly Efficient (≈ 0 dB) Wavelength Conversion Based on Four-Wave Mixing in Quantum Dot Optical Amplifiers. *IEEE Photonic Tech L* **2002**, *14*, 1139–1141.

(12) Kita, T.; Wada, O.; Ebe, H.; Nakata, Y.; Sugawara, M. Polarization-Independent Photoluminescence from Columnar InAs/GaAs Self-Assembled Quantum Dots. *Jpn J Appl Phys* **2002**, *41*, 1143–1145.

(13) Yu, P. et al. Optical Anisotropy in Vertically Coupled Quantum Dots. *Phys Rev B* **1999**, *60*, 680–685.

(14) Kita, T.; Jayavel, P.; Wada, O.; Ebe, H.; Nakata, Y.; Sugawara, M. Polarization Controlled Edge Emission from Columnar InAs/GaAs Self-Assembled Quantum Dots. *Phys Status Solidi (C)* **2003**, *1140*, 1137–1140.

(15) Kita, T.; Tamura, N.; Wada, O.; Sugawara, M.; Nakata, Y.; Ebe, H.; Arakawa, Y. Artificial Control of Optical Gain Polarization by Stacking Quantum Dot Layers. *Appl Phys Lett* **2006**, *88*, 211106.

(16) Usman, M. In-Plane Polarization Anisotropy of Ground State Optical Intensity in InAs/GaAs Quantum Dots. *J Appl Phys* **2011**, *110*, 94512.

(17) Usman, M.; Inoue, T.; Harda, Y.; Klimeck, G.; Kita, T. Experimental and Atomistic Theoretical Study of Degree of Polarization from Multilayer InAs/GaAs Quantum Dot Stacks. *Phys Rev B* **2011**, *84*, 115321.

(18) Usman, M.; Tan, Y. H. M.; Ryu, H.; Ahmed, S. S.; Krenner, H. J.; Boykin, T. B.; Klimeck, G. Quantitative Excited State Spectroscopy of a Single InGaAs Quantum Dot Molecule through Multi-Million-Atom Electronic Structure Calculations. *Nanotech* **2011**, *22*, 315709.

(19) Tillmann, K.; Gerthsen, D.; Pfundstein, P.; Förster, A.; Urban, K. Structural transformations and strain relaxation mechanisms of In0.6Ga0.4As islands grown by molecular beam epitaxy on GaAs(001) substrates. *J Appl Physic* **1995**, *78*, 3824–3832.

(20) Ma, W.; Nötzel, R.; Schönherr, H. P.; Ploog, K. H. Shape transition of coherent three-dimensional (In,Ga)As islands on GaAs(100). *Appl Physic Lett* **2001**, *79*, 4219–4221.

(21) Mano, T.; Nötzel, R.; Hamhuis, G. J.; Eijkemans, T. J.; Wolter, J. H. Effect of annealing on formation of self-assembled (In,Ga)As quantum wires on GaAs (100) by molecular beam epitaxy. *J Appl Physic* **2002**, *92*, 4043–4046.

(22) Hospodková, A.; Křápek, V.; Mates, T.; Kuldová, K.; Pangrác, J.; Hulicius, E.; Oswald, J.; Melichar, K.; Humlíček, J.; Šimeček, T. Lateral shape of InAs/GaAs quantum dots in vertically correlated structures. *J Cryst Growth* **2007**, *298*, 570–573.

(23) Wang, R. H.; Stintz, A.; Varangis, P. M.; Newell, T. C.; Li, H.; Malloy, K. J.; Lester, L. F. Room-temperature operation of InAs quantum-dash lasers on InP [001]. *IEEE Photonic Technol Lett* **2001**, *13*, 767–769.

(24) Ukhanov, A. A.; Wang, R. H.; Rotter, T. J.; Stintz, A.; Lester, L. F.; Eliseev, P. G.; Malloy, K. J. Orientation dependence of the optical properties in InAs quantum-dash lasers on InP. *Appl Physic Lett* **2002**, *81*, 981–983.

(25) Lelarge, F. et al. Recent Advances on InAs/InP Quantum Dash Based Semiconductor Lasers and Optical Amplifiers Operating at 1.55 µm. *IEEE J Sel Top Quantum Electron* **2007**, *13*, 111–124.

(26) Kayanuma, Y. Quantum-size Effects of Interacting Electrons and Holes in Semiconductor Microcrystals with Spherical Shape. *Phys. Rev. B* **1988**, *38*, 9797–9805.

(27) Zhou, D.; Piron, R.; Dontabactouny, M.; Homeyer, E.; Dehaese, O.; Batte, T.; Gicquel, M.; Grillot, F.; Tavernier, K.; Even, J.; Loualiche, S. Effect of stack number on the threshold current density and emission wavelength in quantum dash/dot lasers. *Phys Status Solidi Curr Top Solid State Phys* **2009**, *6*, 2217–2221.

(28) Hein, S.; Podemski, P.; Sęk, G.; Misiewicz, J.; Ridha, P.; Fiore, A.; Patriarche, G.; Höfling, S.; Forchel, A. Orientation dependent emission properties of

columnar quantum dash laser structures. *Appl Phys Lett* **2009**, *94*, 241113(1–3).

(29) Bakonyi, Z.; Su, H.; Onishchukov, G.; Lester, L. F.; Member, S.; Gray, A. L.; Newell, T. C. High-Gain Quantum-Dot Semiconductor Optical Amplifier for 1300 nm. *IEEE J Quant Electron* **2003**, *39*, 1409–1414.

(30) Borri, P.; Schneider, S.; Langbein, W.; Bimberg, D. Ultrafast Carrier Dynamics in InGaAs Quantum Dot Materials and Devices. *J Optic A* **2006**, *8*.

(31) Jayavel, P.; Kita, T.; Wada, O.; Ebe, H.; Sugawara, M.; Arakawa, Y.; Nakata, Y.; Akiyama, T. Optical Polarization Properties of InAs/GaAs Quantum Dot Semiconductor Optical Amplifier. *Jpn J Appl Physic* **2005**, *44*, 2528–2530.

(32) Saito, H.; Nishi, K.; Sugou, S.; Sugimoto, Y. Controlling polarization of quantum-dot surface-emitting lasers by using structurally anisotropic self-assembled quantum dots. *Appl Physic Lett* **1997**, *71*, 590.

(33) Usman, M. Atomistic Theoretical Study of Electronic and Polarization Properties of Single and Vertically Stacked Elliptical InAs Quantum Dots. *Phys Rev B* **2012**, *86*, 155444.

(34) Ben-Ezra, Y.; Haridim, M.; Lembrikov, B. I. Theoretical Analysis of Gain-Recovery Time and Chirp in QD-SOA. *IEEE Photonic Tech L* **2005**, *17*, 1803–1805.

(35) Ben-Ezra, Y.; Lembrikov, B. I.; Haridim, M. Acceleration of Gain Recovery and Dynamics of Electrons in QD-SOA. *IEEE J Quant Electron* **2005**, *41*, 1268–1273.

(36) Li, X.; Li, G. Comments on "Theoretical Analysis of Gain-Recovery Time and Chirp in QD-SOA". *IEEE Photonic Tech L* **2006**, *18*, 2434–2435.

(37) Qasaimeh, O. Characteristics of Cross-Gain (XG) Wavelength Conversion in Quantum Dot Semiconductor Optical Amplifiers. *IEEE Photonic Tech L* **2004**, *16*, 542–544.

(38) Stier, O.; Grundmann, M.; Bimberg, D. Electronic and Optical Properties of Strained Quantum Dots Modeled by 8-Band kp Theory. *Phys Rev B* **1999**, *59*, 5688–5701.

(39) Schliwa, A.; Winkelnkemper, M.; Bimberg, D. Impact of Size, Shape, and Composition on Piezoelectric Effects and Electronic Properties of In(Ga)As/GaAs Quantum Dots. *Phys Rev B* **2007**, *76*, 205324.

(40) Greif, L. A.; Jagsch, S. T.; Wagner, M. R.; Schliwa, A. Tuning the Emission Directionality of Stacked Quantum Dots. *ACS Photonics* **2018**, *5*, 4838–4845.

(41) Zhao, Y.; Han, W.; Song, J.; Li, X.; Liu, Y.; Gao, D.; Du, G.; Cao, H.; Chang, R. P. H. Spontaneous Emission Factor for Semiconductor Superluminescent Diodes. *J Appl Physic* **1999**, *85*, 3945–3948.

(42) Berg, T. W.; Bischoff, S.; Magnusdottir, I.; Moørk, J. Ultrafast Gain Recovery and Modulation Limitations in Self-Assembled Quantum-Dot Devices. *IEEE Photonic Tech L* **2001**, *13*, 541–543.

(43) Uskov, A. V.; Berg, T. W.; Mørk, J. Theory of Pulse-Train Amplification Without Patterning Effects in Quantum-Dot Semiconductor Optical Amplifiers. *IEEE J Quant Electron* **2004**, *40*, 306–320.

(44) Marcuse, D. Computer Model of an Injection Laser Amplifier. *IEEE J Quant Electron* **1983**, *QE-19*, 63–73.

(45) Berg, T. W.; Mørk, J. Saturation and noise properties of quantum-dot optical amplifiers. *IEEE J Quant Electron* **2004**, *40*, 1527–1539.